Multimodal exploitation and sparse reconstruction for guided-wave structural health monitoring

Andrew Golato*, Sridhar Santhanam, Fauzia Ahmad, and Moeness G. Amin
Center for Advanced Communications, College of Engineering, Villanova University,
800 E. Lancaster Ave., Villanova, PA 19085, USA.

ABSTRACT

The presence of multiple modes in guided-wave structural health monitoring has been usually considered a nuisance and a variety of methods have been devised to ensure the presence of a single mode. However, valuable information regarding the nature of defects can be gleaned by including multiple modes in image recovery. In this paper, we propose an effective approach for localizing defects in thin plates, which involves inversion of a multimodal Lamb wave based model by means of sparse reconstruction. We consider not only the direct symmetric and anti-symmetric fundamental propagating Lamb modes, but also the defect-spawned mixed modes arising due to asymmetry of defects. Model-based dictionaries for the direct and spawned modes are created, which take into account the associated dispersion and attenuation through the medium. Reconstruction of the region of interest is performed jointly across the multiple modes by employing a group sparse reconstruction approach. Performance validation of the proposed defect localization scheme is provided using simulated data for an aluminum plate.

Keywords: Sparse reconstruction, multimodal, Lamb waves, compressed sensing, structural health monitoring

1. INTRODUCTION

Structural Health Monitoring (SHM) is a primary technology for the assessment of the integrity of a variety of structures.[1-4] SHM enables self-sensing capabilities in structures, and guided ultrasonic waves within SHM can be used for real-time imaging of defects in thin-walled structures, such as airplanes, bridges, and windmills. Guided ultrasonic waves, such as Lamb waves, can travel large distances without experiencing significant attenuation, and they provide rich interactions with defects. Therefore, they are the preferred wave mode for SHM of thin plate and shell structures.[5-7] Lamb waves are the solutions to the elastic wave equation for a thin plate with traction free surface conditions.[8,9] The solutions are infinite in number and the waves, multimodal by nature, can be separated into symmetric (S) and anti-symmetric (A) modes. While an infinite number of symmetric and anti-symmetric modes exist, the number present in a given structure can be regulated by the frequency of the generated signal. Higher frequencies will offer an overabundance of wave modes, while lower frequencies induce only the fundamental symmetric and anti-symmetric (S_0 and A_0) modes. The phase and group velocities of each individual mode are frequency-dependent, leading to dispersion, which causes the shape of the waves to change during propagation.

Despite the complexity of the propagating Lamb waves, recent advances in computing, processing, and electronics have enabled the exploitation of the information contained in the various modes. Proper utilization of the various modes provides a more robust assessment of the health of the structure as the different modes may contain different information: the S_0 mode is well suited to detecting transverse cracks in the middle of plates, the S_1 mode is biased toward detecting smaller transverse cracks on the surface of plates, and the A_0 and A_1 modes interact strongly with delamination cracks lying in a plane parallel to the plane of the plate.[10]

Recently, the defect imaging problem was cast within the sparse reconstruction framework by recognizing the inherent property that the number of defects is typically much smaller than the number of locations at which a defect could exist.[11, 12] Employing an l_1-norm minimization approach, relatively accurate imaging results were obtained using a single mode in Ref. [11]. More recent work in Ref. [12] accounted for the multimodal nature of Lamb waves by exploiting fundamental symmetric and anti-symmetric modes in unison for scene recovery. However, this multimodal approach did

*agolat01@gmail.com; http://www1.villanova.edu/villanova/engineering/research/centers/cac/facilities/aul.html

not consider the mode conversion phenomenon whereby an asymmetric defect produces both an S_0 and an A_0 wave after interaction with either an A_0 or an S_0 wave.[13] That is, while only two waves, A_0 and S_0, leave a transducer and strike a defect, four corresponding wave modes are received at the receiving transducer, namely, the reflected A_0 and S_0 modes and the two converted modes: the S_0 wave that was spawned at the defect by an A_0 mode and the A_0 wave that was spawned at the defect by an S_0 mode.

In this paper, we present a four-mode multimodal scene reconstruction approach for localizing defects in thin plates. We invert a multimodal Lamb wave based model through exploitation of the sparsity of the defects. We consider model-based dictionaries, one for each of the two excited fundamental modes, which consider the associated dispersion and attenuation through the medium. Additionally, we construct two dictionaries which account for conversion of the excited S_0 and A_0 modes into each other at discontinuities and/or asymmetric defects. Joint recovery of the image of the region of interest (ROI) is performed across all excited and converted modes using the group sparsity constraint.[14-17] We validate the effectiveness of the proposed method through simulated data for an aluminum plate.

The remainder of the paper is organized as follows. In Section 2, we describe the multimodal signal propagation model and present the sparse reconstruction algorithm for exploitation of the multiple fundamental and converted propagating Lamb modes. Supporting simulation results are provided in Section 3. Section 4 presents the concluding remarks.

2. MULTIMODAL SIGNAL MODEL AND SPARSE RECONSTRUCTION

2.1 Signal model

Assume that a network of piezoelectric (PZT) transducers is adhered to the surface of the structure. The transducers are assumed to be employed in a pitch-catch mode for data collection. That is, the transducers work in pairs with one transducer transmitting the signal and the other acting as the receiver. Let there be a total of L unique transmitter-receiver combinations used for interrogating the ROI. The transmitter and receiver corresponding to the lth pair are located at position vectors $\mathbf{t}_l$ and $\mathbf{r}_l$, respectively. Consider P structural defects in the plate. The total received signal corresponding to the lth transmitter-receiver pair is the superposition of the complete set of scattered modes produced by the P defects present and the background signal, and is given by

$$\tilde{\mathbf{z}}_l = \sum_{p=0}^{P-1} (g_{lp,A_0}(t) + g_{lp,S_0}(t) + g_{lp,A_0/S_0}(t) + g_{lp,S_0/A_0}(t)) + b_l(t) \tag{1}$$

where $b_l(t)$ represents the background signal containing both direct path signals and edge reflections for the lth transmitter-receiver pair. The signals $g_{lp,A_0}(t)$, $g_{lp,S_0}(t)$, $g_{lp,A_0/S_0}(t)$, and $g_{lp,S_0/A_0}(t)$ are the received signal components corresponding to the direct and converted modes due to the pth defect when the lth transmitter-pair is active and are defined as the respective inverse Fourier transforms of eqs. (2)-(5).

$$G_{lp,A_0}(f) = x_{p,A_0} H(f) \exp(j2\pi f (\|\mathbf{t}_l - \mathbf{s}_p\|_2 + \|\mathbf{r}_l - \mathbf{s}_p\|_2)/c_{A_0}(f)) \tag{2}$$

$$G_{lp,S_0}(f) = x_{p,S_0} H(f) \exp(j2\pi f (\|\mathbf{t}_l - \mathbf{s}_p\|_2 + \|\mathbf{r}_l - \mathbf{s}_p\|_2)/c_{S_0}(f)) \tag{3}$$

$$G_{lp,A_0/S_0}(f) = x_{p,A_0/S_0} H(f) \exp(j2\pi f (\frac{\|\mathbf{t}_l - \mathbf{s}_p\|_2}{c_{A_0}(f)} + \frac{\|\mathbf{r}_l - \mathbf{s}_p\|_2}{c_{S_0}(f)})) \tag{4}$$

$$G_{lp,S_0/A_0}(f) = x_{p,S_0/A_0} H(f) \exp(j2\pi f (\frac{\|\mathbf{t}_l - \mathbf{s}_p\|_2}{c_{S_0}(f)} + \frac{\|\mathbf{r}_l - \mathbf{s}_p\|_2}{c_{A_0}(f)})) \tag{5}$$

Here, $H(f)$ is the Fourier transform of the excitation waveform $h(t)$, $\mathbf{s}_p$ is the position vector of the pth defect, c_{A_0} and c_{S_0} are the frequency-dependent phase speeds of the A_0 and S_0 modes, respectively, and the parameters x_{p,A_0}, x_{p,S_0}, $x_{p,A_0/S_0}$, and $x_{p,S_0/A_0}$ are the respective scatterer reflectivities under the excited and converted modes. The reflectivities are assumed to be independent of frequency and the aspect angle (angle relative to the transmitter and receiver) of the lth pair.

Note that the model in eq. (1) ignores interactions between the defects Assuming access to the background signals in the absence of the defects permits background subtraction to be performed, which results in a difference signal containing only the defect-scattered waveforms,

$$\mathbf{z}_l = \tilde{\mathbf{z}}_l - b_l(t) = \sum_{p=0}^{P-1} (g_{lp,A_0}(t) + g_{lp,S_0}(t) + g_{lp,A_0/S_0}(t) + g_{lp,S_0/A_0}(t)). \tag{6}$$

The ROI is divided into a uniform grid of M (>> P) pixels, each representing a potential defect location. Let $\mathbf{x}_{A_0}$ and $\mathbf{x}_{S_0}$ represent the lexicographically ordered $M \times 1$ scene reflectivity vectors, corresponding to the spatial sampling grid under the A_0 and S_0 modes, respectively. Similarly, $\mathbf{x}_{A_0/S_0}$ and $\mathbf{x}_{S_0/A_0}$ are the scene reflectivity vectors for the converted modes of the incident A_0 and S_0 modes, respectively. Sampling the lth difference signal $\mathbf{z}_l$ at times $t_k, k = 0,1,..K-1$, yields a $K \times 1$ vector $\mathbf{z}_l$. Using eqs. (2)-(6), the linear relationship between the lth difference signal and the scene reflectivity vectors can be obtained as

$$\mathbf{z}_l = \mathbf{\Psi}_{l,A_0}\mathbf{x}_{A_0} + \mathbf{\Psi}_{l,S_0}\mathbf{x}_{S_0} + \mathbf{\Psi}_{l,A_0/S_0}\mathbf{x}_{A_0/S_0} + \mathbf{\Psi}_{l,S_0/A_0}\mathbf{x}_{S_0/A_0} \tag{7}$$

where $\mathbf{\Psi}_{l,A_0}$, $\mathbf{\Psi}_{l,S_0}$, $\mathbf{\Psi}_{l,A_0/S_0}$, and $\mathbf{\Psi}_{l,S_0/A_0}$ are the dictionary matrices corresponding to the direct and the converted modes, each of dimension $K \times M$. The mth column of $\mathbf{\Psi}_{l,A_0}$ consists of the scattered A_0 wave that corresponds to a defect at the mth grid-point $\mathbf{s}_m$ where the kth element of the mth column is given by

$$[\mathbf{\Psi}_{l,A_0}]_{k,m} = F^{-1}\left\{H(f)\exp(j2\pi f(\|\mathbf{t}_l - \mathbf{s}_m\|_2 + \|\mathbf{r}_l - \mathbf{s}_m\|_2)/c_{A_0}(f))\right\}_{t=t_k}. \tag{8}$$

The mth column of $\mathbf{\Psi}_{l,S_0}$ consists of the scattered S_0 wave corresponding to a defect at $\mathbf{s}_m$ with its kth element expressed as

$$[\mathbf{\Psi}_{l,S_0}]_{k,m} = F^{-1}\left\{H(f)\exp(j2\pi f(\|\mathbf{t}_l - \mathbf{s}_m\|_2 + \|\mathbf{r}_l - \mathbf{s}_m\|_2)/c_{s_0}(f))\right\}_{t=t_k}. \tag{9}$$

In a similar manner, the (k, m)th elements of the converted mode dictionary matrices are expressed as

$$[\mathbf{\Psi}_{l,S_0/A_0}]_{k,m} = F^{-1}\left\{H(f)\exp(j2\pi f(\frac{\|\mathbf{t}_l - \mathbf{s}_m\|_2}{c_{S_0}(f)} + \frac{\|\mathbf{r}_l - \mathbf{s}_m\|_2}{c_{A_0}(f)}))\right\}_{t=t_k} \tag{10}$$

$$[\mathbf{\Psi}_{l,A_0/S_0}]_{k,m} = F^{-1}\left\{H(f)\exp(j2\pi f(\frac{\|\mathbf{t}_l - \mathbf{s}_m\|_2}{c_{A_0}(f)} + \frac{\|\mathbf{r}_l - \mathbf{s}_m\|_2}{c_{s_0}(f)}))\right\}_{t=t_k}. \tag{11}$$

While eq. (7) only considers the contribution of a single transmitter-receiver pair, the measured data vector $\mathbf{z}$ for all L transmitter-receiver combinations is obtained simply by stacking all L difference signal vectors into a single column vector $\mathbf{z} = \left[\mathbf{z}_0^T \quad \mathbf{z}_1^T \quad \cdots \quad \mathbf{z}_{L-1}^T\right]^T$ of dimension $KL \times 1$, given by

$$\mathbf{z} = \mathbf{\Psi}_{A_0}\mathbf{x}_{A_0} + \mathbf{\Psi}_{S_0}\mathbf{x}_{S_0} + \mathbf{\Psi}_{A_0/S_0}\mathbf{x}_{A_0/S_0} + \mathbf{\Psi}_{S_0/A_0}\mathbf{x}_{S_0/A_0} \tag{12}$$

where the superscript 'T' denotes the matrix transpose operation and

$$\mathbf{\Psi}_{\Lambda} = \left[\mathbf{\Psi}_{0,\Lambda}^{\mathbf{T}} \quad \mathbf{\Psi}_{1,\Lambda}^{\mathbf{T}} \quad \cdots \quad \mathbf{\Psi}_{L-1,\Lambda}^{\mathbf{T}}\right]^{\mathbf{T}} \text{ for } \Lambda = A_0, S_0, S_0/A_0, A_0/S_0 \tag{13}$$

is the dictionary matrix of size $KL \times M$. Note that if downsampling in the time and/or spatial domains is desired, it can be incorporated into the signal model simply by premultiplying $\mathbf{z}$ by a downsampling matrix Φ. Details on the design of the matrix Φ can be found in Ref. [18].

2.2 Group sparse reconstruction

Although the direct fundamental symmetric and anti-symmetric modes and the two converted modes have different defect reflectivities, the corresponding reflectivity vectors share a common sparsity pattern. That is, if a particular element of $\mathbf{x}_{A_0}$ is nonzero, then so must be the corresponding elements of $\mathbf{x}_{S_0}$, $\mathbf{x}_{A_0/S_0}$, and $\mathbf{x}_{S_0/A_0}$, since the elements are representing the same location in the same scene. As such, a group sparse reconstruction approach is applied as follows. The reflectivity vectors $\mathbf{x}_{A_0}$, $\mathbf{x}_{S_0}$, $\mathbf{x}_{A_0/S_0}$, and $\mathbf{x}_{S_0/A_0}$ are stacked to form a single $4M \times 1$ vector $\mathbf{x} = \begin{bmatrix} \mathbf{x}_{A_0}^{\mathbf{T}} & \mathbf{x}_{S_0}^{\mathbf{T}} & \mathbf{x}_{A_0/S_0}^{\mathbf{T}} & \mathbf{x}_{S_0/A_0}^{\mathbf{T}} \end{bmatrix}^{\mathbf{T}}$. The measurement vector, $\mathbf{z}$, can then be expressed as

$$\mathbf{z} = \boldsymbol{\Psi}\mathbf{x} \tag{14}$$

where $\boldsymbol{\Psi} = \begin{bmatrix} \boldsymbol{\Psi}_{A_0} & \boldsymbol{\Psi}_{S_0} & \boldsymbol{\Psi}_{A_0/S_0} & \boldsymbol{\Psi}_{S_0/A_0} \end{bmatrix}$ is a composite dictionary matrix of dimension $KL \times 4M$. The scene vector $\mathbf{x}$ exhibits a group sparse structure, whereby the group extends across the four considered modes for each pixel location. The vector $\mathbf{x}$, can be recovered from the measurements $\mathbf{z}$ through either a mixed l_2/l_1 norm optimization,[19]

$$\hat{\mathbf{x}} = \arg\min_x \frac{1}{2}\|\mathbf{z} - \boldsymbol{\Psi}\mathbf{x}\|_2^2 + \lambda\|\mathbf{x}\|_{2,1}, \tag{15}$$

where $\|\mathbf{x}\|_{2,1} = \sum_{m=0}^{M-1} \left\| \begin{bmatrix} \hat{x}_{m,A_0} & \hat{x}_{m,S_0} & \hat{x}_{m,A_0/S_0} & \hat{x}_{m,S_0/A_0} \end{bmatrix}^T \right\|_2$ and λ is a regularization parameter, or a block version of the Orthogonal Matching Pursuit algorithm (BOMP).[20] In this work, BOMP is preferred for scene recovery.

Once the recovered vector $\hat{\mathbf{x}}$ has been obtained, the individual reflectivity vectors $\hat{\mathbf{x}}_\Lambda$, $\Lambda = A_0, S_0, A_0/S_0, S_0/A_0$, contained within $\hat{\mathbf{x}}$, are combined to obtain a single composite scene representation $\tilde{\mathbf{x}}$ by simply calculating the l_2 norm across the elements of these vectors as[19]

$$[\tilde{\mathbf{x}}]_{\mathbf{m}} = \tilde{x}_m = \left\| \begin{bmatrix} \hat{x}_{m,A_0} & \hat{x}_{m,S_0} & \hat{x}_{m,A_0/S_0} & \hat{x}_{m,S_0/A_0} \end{bmatrix}^T \right\|_2. \tag{16}$$

3. SIMULATION RESULTS

3.1 Simulation parameters and setup

Let the simulation environment consist of a 3.12 mm thick aluminum plate, whose square base dimension is 1.22 m. A network of five transducers is attached to its surface, at the locations shown in Fig. 1, which provide a total of $L = 10$ transmitter-receiver combinations. The transducers are excited with a Hanning-windowed, five-cycle burst of a 150 kHz sinusoidal signal. Let the ROI be a 400 mm square area at the center of the plate surface. This choice ensures that the plate boundaries are sufficiently far from the transducers; therefore, boundary reflections are considered insignificant and not included in the simulated data. The ROI is divided into a 31×31 pixel-grid resulting in a total of $M = 961$ pixels. The sampling rate is 1 MHz, which results in $K = 400$ recorded samples over a time interval of 400 μs. The resultant measurement vector has a length of 4000. The individual dictionaries corresponding to the direct and converted modes have a dimension of 4000×961 each; thus, the composite multimodal dictionary in eq. (14) has dimensions 4000×3844.

Consider two defects, both modeled as point scatterers. The first defect is located at (160,160) mm and is assumed to interact strongly with the incident A_0 mode (reflectivities are set to $x_{0,A_0} = 1.0$ and $x_{0,s_0} = 0.1$). The second defect is located at (340,340) mm, and similarly biases the incident S_0 mode (reflectivities are $x_{1,A_0} = 0.1$ and $x_{1,S_0} = 1.0$). The two converted modes are assumed to be spawned with equal strength by the defects, such that the converted mode reflectivities are set to $x_{0,S_0/A_0} = x_{1,S_0/A_0} = x_{0,A_0/S_0} = x_{1,A_0/S_0} = 0.5$. White Gaussian noise with a signal-to-noise ratio (SNR) of 10 dB is added to the simulated measurements. While 10 distinct transmitter-receiver pairings exist, spatial downsampling is considered, according to which measurements from only 5 randomly chosen transmitter-receiver pairs

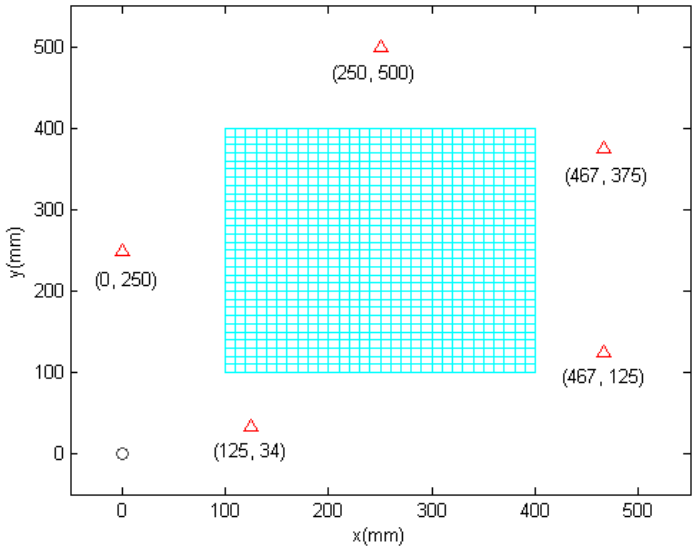

Figure 1. Schematic of the simulation setup. Red triangles represent transducers with coordinates listed in millimeters. Blue mesh-grid represents the pixelized ROI. All coordinates are relative to the coordinate system displayed with origin indicated by the circle in lower left-hand corner.

are utilized in the reconstruction. The resultant spatially downsampled measurement vector consists of only 2000 samples and the individual dictionaries corresponding to each of the four modes have dimensions 2000×961, while the composite multimodal dictionary is of size 2000×3844.

The first attempt at scene recovery employs single-mode based sparse scene recovery for the A_0 and S_0 modes individually. Orthogonal matching pursuit (OMP)[21] reconstructs the corresponding reflectivity vectors $\mathbf{x}_{S_0}$ and $\mathbf{x}_{A_0}$ by considering the individual single-mode linear signal models $\mathbf{z} = \boldsymbol{\Psi}_{S_0}\mathbf{x}_{S_0}$ and $\mathbf{z} = \boldsymbol{\Psi}_{A_0}\mathbf{x}_{A_0}$, respectively, after premultiplication by the appropriate downsampling matrix. This reconstruction process is repeated 100 times, where a different randomly selected set of 5 transmitter-receiver pairs is chosen per trial run. The number of OMP iterations in each case was set to 2. The results of the single-mode sparse reconstruction simulation, averaged over the 100 Monte Carlo runs, are shown in Figs. 2(a) and 2(b) for the A_0 and S_0 modes, respectively. The image intensity in each figure is such that the maximum intensity value is normalized to 0 dB. As expected, each single-mode reconstruction can confidently detect and localize only one of the two defects.

Next, the proposed 4 mode multimodal approach, which utilizes the direct and converted modes, is employed for scene reconstruction. Two iterations of BOMP are employed for the group sparse recovery of the multimodal target reflectivity vector. As in the single-mode reconstruction, the multimodal reconstruction is repeated 100 times with the averaged result shown in Fig. 3(b). For comparison, Fig. 3(a) displays the multimodal reconstruction results while ignoring the two converted modes. Fig. 3 clearly demonstrates that the multimodal approach provides superior performance over the single mode reconstructions as it properly detects and localizes both defects. Furthermore, the multimodal result with the inclusion of the converted modes provides a 'cleaner' image compared to the one that ignores them.

4. CONCLUSION

This work proposed a sparse reconstruction approach for detecting defects in thin plates, which exploited the directly scattered fundamental symmetric and anti-symmetric Lamb modes as well as defect spawned converted modes by imposing a block sparse structure across the modes. Model-based dictionaries accounting for the associated dispersion and attenuation through the medium were constructed for the four modes Simulation results validated the proposed approach by exposing the shortcomings of single mode only reconstructions and highlighting the superior performance of the 4-mode multimodal block reconstruction approach.

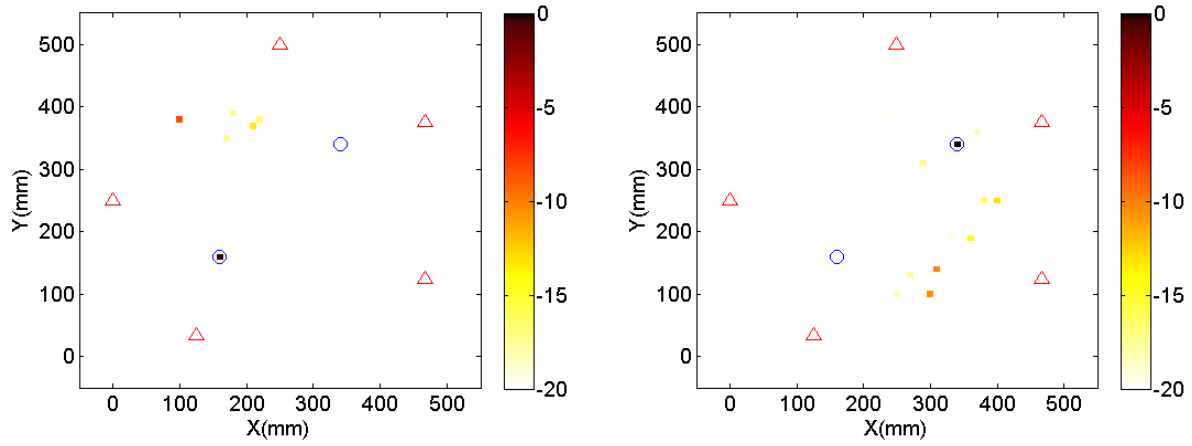

(a) (b)

Figure 2 shows the results of the single-mode sparse reconstructions using OMP for the A_0 mode (a) and the S_0 mode (b) individually. The true defect locations are located by blue circles and the transducer locations are represented by red triangles.

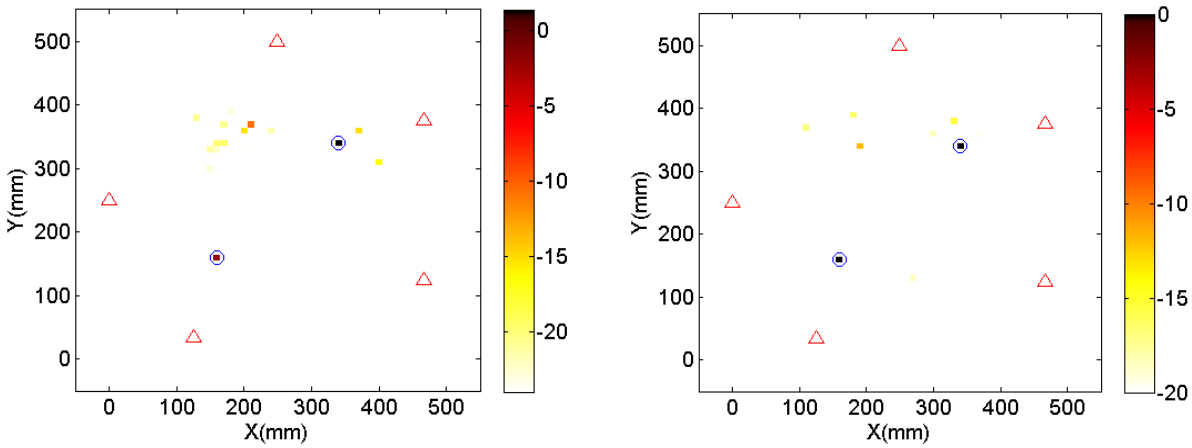

(a) (b)

Figure 3 displays the multimodal reconstruction using BOMP. Blue circles denote the correct defect locations while the red triangles mark the transducer locations. (a) Employs just the two fundamental modes, while (b) exploits four modes by using the converted modes and the fundamental modes.

ACKNOWLEDGMENT

This research is supported in part by the National Science Foundation (NSF) under grant number IIP-0917690.

REFERENCES

[1] Kessler, S. S., Spearing, S. M. and Soutis, C., "Structural health monitoring in composite materials using Lamb wave methods," *Smart Materials and Structures* 11(2), 269-278 (2002).

[2] Raghavan, A. and Cesnik, C. E. S., "A review of guided wave structural health monitoring," *Shock and Vibrations Digest* 39(2), 91-114 (2007).

[3] Giurgiutiu, V. and Santoni-Bottai, G., "Structural health monitoring of composite structures with piezoelectric wafer active sensors," *AIAA Journal* 49(3), 565-581 (2011).

[4] Santhanam, S. and Demirli, R., "Reflection and transmission of fundamental Lamb wave modes obliquely incident on a crack in a plate," *Proc. IEEE Int. Ultrasonics Symp.*, 2690-2693 (2012).

[5] Ramadas, C., Balasubramaniam, K., Joshi, M., and Krishnamurthy, C., "Interaction of the primary antisymmetric Lamb mode with the symmetric delaminations: numerical and experimental studies," *Smart Mater. Struct.* 18(1), 1-7 (2009).

[6] Sohn, H., Park, G., Walt, J., Limback, N. P. and Farrar, C., "Wavelet based active sensing for delamination detection in composite structures," *Smart Mater. Struct.* 13(1), 153-160 (2004).

[7] Tua, P., Quek, S. and Wang, Q., "Detection of cracks in plates using piezo-actuated Lamb waves," *Smart Mater. Struct.* 13(1), 643-660 (2004).

[8] Achenbach, J., [Wave Propagation in Elastic Solids], North Holland, New York (1984).

[9] Rose, J., [Ultrasonic Waves in Solid Media], Cambridge University Press, Cambridge, UK (1999).

[10] Ng, C. and Veidt, M., "Scattering of the fundamental antisymmetric Lamb wave at delaminations in composite laminates," *J. Acoust. Soc. Am.* 129(1), 1288-1296 (2011).

[11] Levine, R. M. and Michaels, R. M., "Model-based imaging of damage with Lamb waves via sparse reconstruction," *J. Acoust. Soc. Am.* 133(3), 1525-1534 (2013).

[12] Golato, A., Santhanam, S., Ahmad, F., and Amin, M. G., "Multimodal sparse reconstruction in Lamb wave-based structural health monitoring," Proc. SPIE Vol. 9109, 91090P (2014).

[13] Golato, A., Santhanam, S., Ahmad, F., and Amin, M. G., " Multimodal Sparse Reconstruction in Lamb Wave Based Defect Localization in Thin Plates," *Structural Health Monitoring*, under review (2014).

[14] Yuan, M. and Lin, Y., "Model selection and estimation in regression with grouped variables," J. *Royal Stat. Soc. Series B* 68(1), 49–67 (2007).

[15] Eldar, Y. C., Kuppinger, P. and Bolcskei, H., "Block-sparse signals: Uncertainty relations and efficient recovery," *IEEE Trans. Signal Process*. 58(6), 3042–3054 (2010).

[16] Leigsnering, M., Ahmad, F., Amin, M. and Zoubir, A., "Compressive sensing based specular multipath exploitation for through-the-wall radar imaging," *Proc. IEEE Int. Conf. Acoust., Speech, Signal Process.*, 6004-6008 (2013).

[17] Amin, M. G. and Ahmad, F., "Compressive sensing for through-the-wall radar imaging," *J. Electron. Imaging.* 22(3), 030901 (2013).

[18] Qian, J., Ahmad, F. and Amin, M.G. , "Joint localization of stationary and moving targets behind walls using sparse scene recovery," *J. Electronic Imaging*, 2013, 22(2), 021002.

[19] Leigsnering, M., Ahmad, F., Amin, M. and Zoubir, A., "Multipath exploitation in through-the-wall radar imaging using sparse reconstruction," *IEEE Trans.Aerosp. Electronic Syst.*, 2014, 50(2), 920-939.

[20] Eldar, Y.C., Kuppinger, P. and Bolckei, H., "Block-sparse signals: Uncertainty relations and efficient recovery," *IEEE Trans. Signal Process.*, 2010, 58, 3042-3054.

[21] Tropp, J. A. and Gilbert, A.C., "Signal recovery from random measurements via orthogonal matching pursuit," *IEEE Trans. Inf. Theory*, 2007, 53(12), 4655–4666.